Cell Reports

Vesicular Glutamate Transporters (SLCA17 A6, 7, 8) Control Synaptic Phosphate Levels

Graphical Abstract

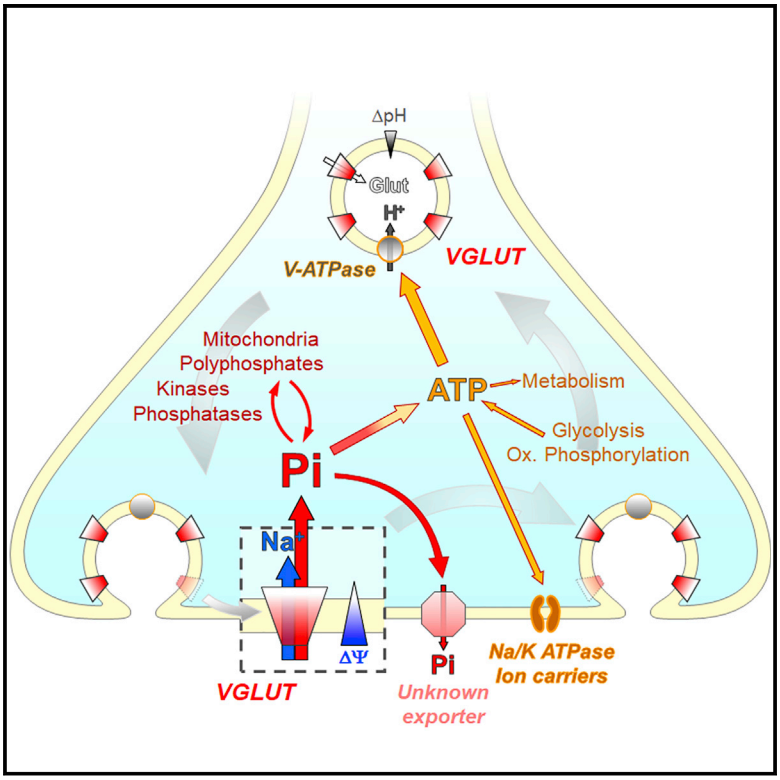

Authors

Cyril Cheret, Marcelo Ganzella, Julia Preobraschenski, Reinhard Jahn, Gudrun Ahnert-Hilger

Correspondence

rjahn@gwdg.de (R.J.),
gahnert@gwdg.de (G.A.-H.)

In Brief

Cheret et al. show that vesicular glutamate transporters that are essential for glutamatergic neurotransmission function as potent NaPi transporters when integrated into the plasma membrane during exocytosis. VGLUTs counteract Pi loss and maintain Pi homeostasis in presynaptic terminals required to sustain intracellular processes.

Highlights

- All vesicular glutamate transporters (VGLUTs) transport NaPi when in the plasma membrane
- VGLUTs play a role in sustaining cytoplasmic Pi levels in presynaptic terminals
- VGLUTs mediate NaPi transport in neurons following stimulation
- Transport of glutamate and Pi is mediated by an overlapping binding site

Cheret et al., 2021, Cell Reports *34*, 108623
January 12, 2021
https://doi.org/10.1016/j.celrep.2020.108623

Cell Reports

CellPress
OPEN ACCESS

Report

Vesicular Glutamate Transporters (SLCA17 A6, 7, 8) Control Synaptic Phosphate Levels

Cyril Cheret,[1,3] Marcelo Ganzella,[2] Julia Preobraschenski,[2,4,5] Reinhard Jahn,[2,6,*] and Gudrun Ahnert-Hilger[1,2,6,7,*]
[1]Institute for Integrative Neuroanatomy, Charité, Medical University of Berlin, 10115 Berlin, Germany
[2]Laboratory of Neurobiology, Max-Planck-Institute for Biophysical Chemistry, and University of Göttingen, 37077 Göttingen, Germany
[3]Present address: Berlin Institute of Health, 10115 Berlin, Germany
[4]Present address: Cluster of Excellence "Multiscale Bioimaging: from Molecular Machines to Networks of Excitable Cells" (MBExC), University of Göttingen, 37077 Göttingen, Germany
[5]Present address: Institute for Auditory Neuroscience, University Medical Center Göttingen, 37077 Göttingen, Germany
[6]These authors contributed equally
[7]Lead Contact
*Correspondence: rjahn@gwdg.de (R.J.), gahnert@gwdg.de (G.A.-H.)
https://doi.org/10.1016/j.celrep.2020.108623

SUMMARY

Vesicular glutamate transporters (VGLUTs) fill synaptic vesicles with glutamate. VGLUTs were originally identified as sodium-dependent transporters of inorganic phosphate (Pi), but the physiological relevance of this activity remains unclear. Heterologous expression of all three VGLUTs greatly augments intracellular Pi levels. Using neuronal models, we show that translocation of VGLUTs to the plasma membrane during exocytosis results in highly increased Pi uptake. VGLUT-mediated Pi influx is counteracted by Pi efflux. Synaptosomes prepared from perinatal VGLUT2$^{-/-}$ mice that are virtually free of VGLUTs show drastically reduced cytosolic Pi levels and fail to import Pi. Glutamate partially competes with sodium (Na^+)/Pi (NaPi)-uptake mediated by VGLUTs but does not appear to be transported. A nanobody that blocks glutamate transport by binding to the cytoplasmic domain of VGLUT1 abolishes Pi transport when co-expressed with VGLUT1. We conclude that VGLUTs have a dual function that is essential for both vesicular glutamate loading and Pi restoration in neurons.

INTRODUCTION

Neuronal communication is mediated by the exocytosis of neurotransmitters stored in synaptic vesicles (SV) of presynaptic nerve endings. After endocytosis, SVs are pre-loaded with neurotransmitters by specific secondary active transporters depending on an electrochemical proton gradient ($\Delta\mu H^+$) across the vesicle membrane, generated by a vacuolar proton pump (V-ATPase).

Loading of SVs with glutamate, the major excitatory neurotransmitter of the mammalian central nervous system (CNS), is mediated by vesicular glutamate transporters (VGLUTs) 1, 2, and 3 that are differentially expressed in the mammalian CNS (Anne and Gasnier, 2014; Edwards, 2007). VGLUT1 and 2 are essential for neurotransmission in all glutamatergic neurons (Gras et al., 2008; Moechars et al., 2006; Seal et al., 2008; Wojcik et al., 2004). VGLUT3 is expressed in the sensory inner hair cells (Seal et al., 2008) and in various non-glutamatergic neurons, where it contributes to vesicular uptake of other transmitters (El Mestikawy et al., 2011; Münster-Wandowski et al., 2016; Seal et al., 2008).

VGLUTs operate as electrogenic glutamate importers during the initial phase of SV loading, with the negative charge being balanced by protons pumped in by the V-ATPase (Eriksen et al., 2016; Juge et al., 2010; Martineau et al., 2017; Preobraschenski et al., 2014). Once the buffering capacity of the SV lumen is exhausted, protons exit the vesicle by a VGLUT-dependent proton-potassium exchange activity (Preobraschenski et al., 2014). A sodium-proton exchanger (NHE6) may provide another exit pathway for protons (Nakamura et al., 2005; Preobraschenski et al., 2014).

Despite their central function in loading SVs with glutamate, VGLUT1 and 2 harbor a second transport activity that is difficult to reconcile with their critical role in neurotransmission. Indeed, both transporters were originally identified as Na^+-coupled transporters for inorganic phosphate (Pi) (Aihara et al., 2000; Ni et al., 1994), although their essential function in glutamate loading of SVs was recognized later (Bellocchio et al., 2000; Hayashi et al., 2001; Takamori et al., 2000, 2001, 2002). VGLUTs are structurally related to ubiquitously expressed NaPi transporters type I that together constitute a subfamily of solute carriers (SLC17A) (Reimer, 2013; Reimer and Edwards, 2004). Biochemical studies using purified VGLUTs reconstituted in artificial membranes have confirmed that transport activities for glutamate and Pi reside in the same molecules (Juge et al., 2006; Preobraschenski et al., 2018). Recently, we have shown that the substrate binding sites overlap, with glutamate being the preferred substrate in the cytoplasmic orientation and Pi having

a higher affinity for the transporter in the luminal/extracellular orientation (Preobraschenski et al., 2018). However, it is still mysterious as to whether the NaPi transport activity of VGLUTs contributes to the neuronal Pi balance in a physiologically relevant manner or whether, under physiological conditions, Pi is mainly recovered by established phosphate transporters, such as Pi transporter (PiT) 1 and PiT2 present in neurons and astrocytes (Chande and Bergwitz, 2018; Inden et al., 2016).

Here, we set out to clarify whether VGLUTs are indeed major players in regulating intracellular Pi concentrations in neurons. Although VGLUTs are characterized by a predominantly intracellular localization, they recycle via exo- and endocytosis, spending time in the plasma membrane. Indeed, we have recently shown that heterologous expression of VGLUT1 in secretory vesicles of PC12 cells results in VGLUT-mediated Na^+-dependent Pi uptake that is increased when exocytosis is stimulated (Preobraschenski et al., 2018). Using a combination of VGLUT-transfected cell lines and neuronal models, we now show that all three VGLUTs are potent Na^+-dependent Pi transporters that play a role in sustaining cytoplasmic Pi homeostasis.

RESULTS

VGLUT1, 2, and 3 Are NaPi Transporters

Expression of VGLUT1 in PC12 cells significantly increased the intracellular Pi concentration, which was Na^+ dependent and sensitive to VGLUT inhibitors, as shown previously (Preobraschenski et al., 2018). This also applies to VGLUT2 and 3, as seen with several cell lines that stably express each of the three VGLUT proteins, as confirmed by immunohistochemistry (IHC) (Figures 1A, S1A, and S1B). Expression of each VGLUT protein comparably increased cellular Pi content (depolarization dependent: PC12 or independent: COS7 and HEK293A cells) when the cells were incubated in Pi-containing buffers after a period of Pi starvation. Pi increases depended on Na^+ and were sensitive to the VGLUT inhibitors Rose bengal (RB) or Evans blue (EB) added during the final uptake step (Figures 1A and S1). Thus, all three VGLUTs are potent NaPi transporters.

VGLUTs Are Regulators of the Intracellular Pi Balance in Neurons

To investigate whether endogenous VGLUTs are involved in regulating Pi levels in neurons, we preincubated primary neurons in culture in Pi-free KREBS buffers, followed by an incubation in Pi-containing uptake buffer to monitor Pi reloading. Under non-depolarizing conditions, intracellular Pi content slightly increased abolished by RB added during uptake (Figure 1B). When exocytosis of VGLUT-containing SVs was stimulated by $[K^+]$ depolarization, intracellular Pi increased more than 2-fold in a RB-sensitive manner (Figure 1B). Depolarization in the absence of external Pi did not alter resting cytosolic Pi levels (Figure S2A). Because VGLUTs are highly concentrated in synapses, we repeated the experiments using synaptosomes prepared from adult rat brain. Again, we observed significant NaPi uptake following depolarization, which was sensitive to VGLUT inhibition by RB (Figure 1C, left).

To learn more about the role of VGLUTs for the dynamic equilibrium of Pi concentration, we incubated synaptosomes in KREBS buffers containing 10 mM [Pi] and measured cytoplasmic versus extracellular Pi levels 2 or 15 min after synaptosomes were transferred to a Pi-free uptake buffer. As a result, a considerable Pi efflux was observed, reaching 30% after 2 min and 60% within 15 min. When RB was present, net Pi efflux increased rather than decreased, suggesting that efflux is continuous and independent of VGLUT. The intra-synaptosomal Pi content decreased in parallel (Figure S2B, right). Note that the intra-synaptosomal content was about 3- to 4-fold higher in synaptosomes that were incubated with Pi after a period of Pi starvation than in synaptosomes maintained in Pi-free buffer (Figure S2B). We conclude that, in neurons and synaptic terminals, VGLUT-mediated NaPi transport activity is essential for maintaining cytoplasmic Pi levels.

To confirm the relevance of VGLUTs for the synaptic Pi balance, we measured Pi content and Pi efflux of synaptosomes derived from VGLUT2$^{-/-}$ mice. Prenatally, VGLUT2 is the main transporter in brain, while VGLUT1 expression increases postnatally (Boulland et al., 2004). Homozygous VGLUT2$^{-/-}$ mice die at birth (Moechars et al., 2006; Wallén-Mackenzie et al., 2006) with no major morphological aberrations in their brains (Wallén-Mackenzie et al., 2006), providing an opportunity to analyze Pi regulation in synapses devoid of VGLUTs.

First, we verified the developmental profile of VGLUT expression reported previously (Boulland et al., 2004) using synaptosomes isolated from embryonic day 18 (E18) and early postnatal brains. VGLUT2 was clearly detectable in wild-type (WT) mice at E18 and increased during the first postnatal days although VGLUT1 or VGLUT3 expression only became apparent in adults (Figure 2A, left panel). The SV markers synaptophysin and SV2A steadily increased, highlighting synaptogenesis (Becher et al., 1999; Marazzi and Buckley, 1993). The Pi transporters PiT1 and PiT2 were expressed at all developmental stages (Inden et al., 2016).

When comparing the expression profile of these proteins in E18 synaptosomes derived from VGLUT2$^{-/-}$ (WT, heterozygous, and homozygous) littermates, only VGLUT2 expression was lost although the other tested synaptic proteins (with the exception of PiT2) did not change (Figure 2A, right panel). With no compensatory expression of VGLUT1 or VGLUT3, synaptosomes prepared at E18 from VGLUT2$^{-/-}$ mice lack all VGLUTs.

Next, synaptosomes from the VGLUT2$^{-/-}$ strain were depolarized and preincubated in Pi-free KREBS buffers and then shifted to Pi-free or Pi-containing uptake buffers as described above, followed by measuring Pi content. As shown in Figure 2B, Pi content was reduced in synaptosomes derived from heterozygous and even further decreased in synaptosomes derived from homozygous mice. Application of 10 mM [Pi] in the extracellular milieu increased Pi content in both WT and heterozygous, but not in homozygous synaptosomes (Figures 2B and 2C, left panel). In the presence of the VGLUT inhibitor RB, Pi in all genotypes reached levels displayed by synaptosomes from VGLUT2$^{-/-}$ homozygous mice under all tested conditions. Thus, a potent Pi efflux takes place in embryonic synaptosomes, which is counteracted by VGLUT2 activity even in the nominal absence of extracellular Pi (Figure 2C, right panel). This Pi restoration is hardly visible when VGLUT2 is deleted or inhibited by RB reaching minimal resting Pi value in the absence of VGLUT

CellPress
OPEN ACCESS

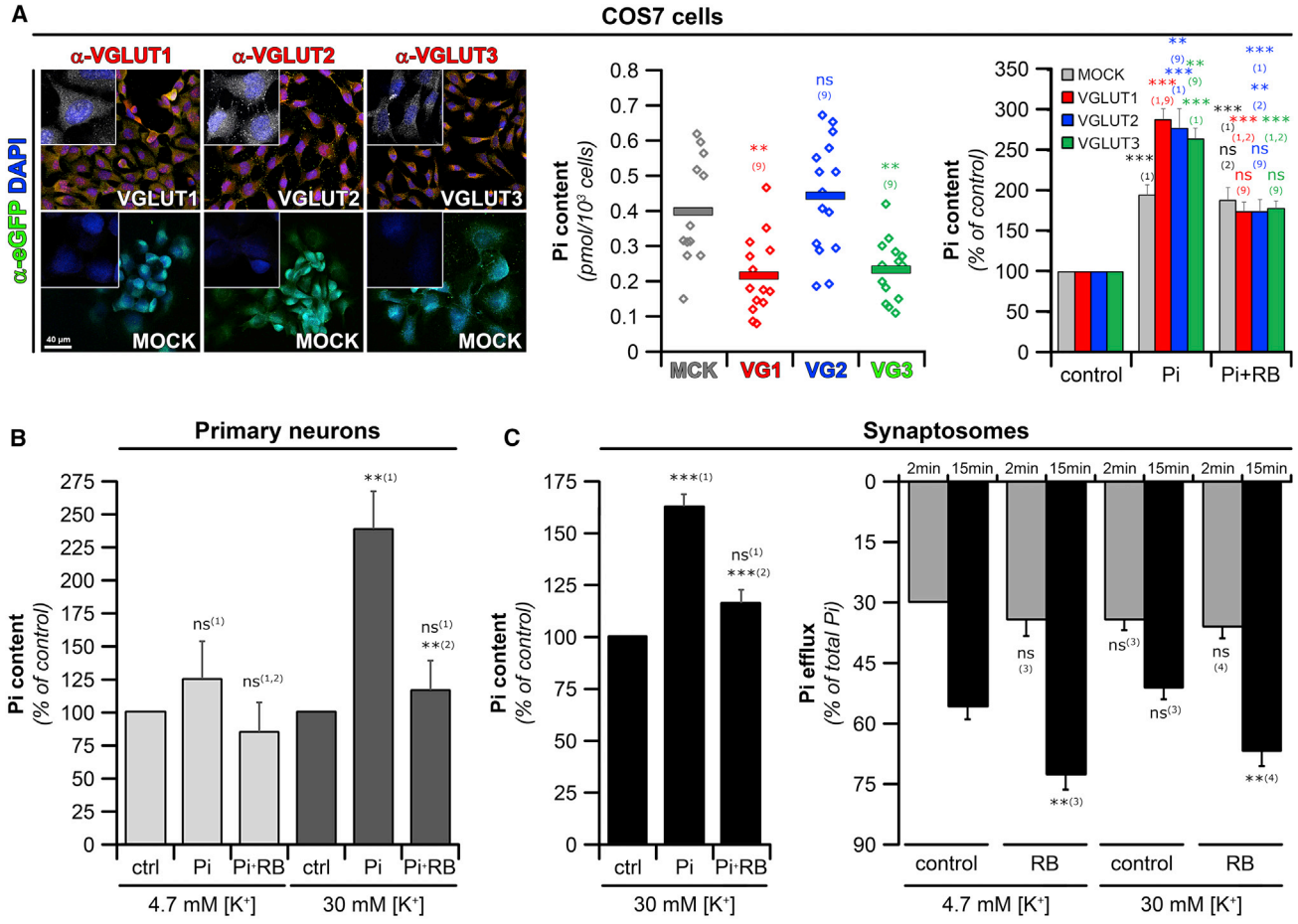

Figure 1. VGLUT-1, -2, or -3 Increase Pi Transport

(A) COS7 cells. (Left) VGLUT-1, -2, and -3 are detected in the respective COS7 subclones expressing VGLUT-IRES-EGFP constructs and not in the MOCK clone expressing only EGFP. (Insets) Twice magnified cells are labeled with DAPI (blue) and the respective VGLUT variant (white). Scale bar, 40 µm. (Middle) Pi concentrations in control condition (Pi starvation in KREBS 4.7 mM [K^+] followed by 15 min incubation in Pi-free uptake buffer) given as pmol Pi/10^3 cells were comparable between the different COS7 clones. (Right) Pi content of COS7-VGLUTs cells incubated in uptake buffer containing no or 10 mM [Pi] ± 10 µM Rose bengal (RB) is shown. Values were normalized to the controls (no Pi in all incubation steps; see values in middle panel). Mean values ± SEM; n ≥ 10.

(B) Neuronal preparations. (Left) Cultured primary neurons were preincubated for 1 h in Pi-free KREBS 4.7 mM [K^+]. One batch of cells was then depolarized with Pi-free KREBS 30 mM [K^+] and 80 µM Dynasore to prevent endocytosis. After washing in Pi-free KREBS 4.7 mM [K^+], neurons were incubated for 15 min in uptake buffer ± 10 mM [Pi] ± 10 µM [RB]. The presence of Pi caused a RB-sensitive increase in cellular Pi content (light gray bars) that was augmented when cells were first depolarized to induce exocytosis (dark gray bars). Stimulation did not change resting cytoplasmic Pi concentrations (Figure S2A). (Middle) Pi content of synaptosomes from adult rat brains after successive depolarization, repolarization (Pi free buffer), and incubation in uptake buffer ± 10 mM [Pi] ± 10 µM [RB] steps (see STAR Methods). The presence of Pi increased synaptosomal Pi content in a RB-sensitive manner. (Right) Synaptosomes subjected to incubation and repolarization using KREBS buffer containing either 30 or 4.7 mM [K^+] plus 10 mM Pi were analyzed after either 2- or 15-min incubation in Pi-free uptake buffer ± RB. Pi efflux increased with time and was enhanced by RB. The intracellular content decreased correspondingly (Figure S2B, right).

Data show mean values ± SEM given as % of Pi content observed in Pi-free control (left and middle, samples presented with no Pi) or as % of total Pi (extracellular and cytoplasmic, right) from at least 4 (left), 14 (middle), or 3 (right) preparations. Significance toward: (1) no Pi added; (2) Pi; (3) 4.7 mM [K^+] control; (4) 30 mM [K^+] control; and (9) MOCK.

activity. These data indicate that VGLUTs are crucial for synaptic Pi homeostasis.

NaPi and H^+/Glutamate Transport Activities of VGLUTs Are Connected at the Molecular Level

Next, we investigated the relation between the two different transport activities of VGLUTs. First, we examined whether extracellular glutamate competes with VGLUT-dependent Pi loading. Second, we tested whether a nanobody shown earlier to inhibit H^+-dependent glutamate uptake by binding to the cytoplasmic domain of VGLUT1 also affects its NaPi transport activity.

Glutamate clearly inhibited NaPi transport in both COS7- and HEK293A-VGLUT cell lines, irrespective of the VGLUT variant (apparent Ki in COS7 cells for VGLUT1/2/3: 1.37/1.47/0.96 mM glutamate, respectively; Figures 3A, left, and S3A), confirming our previous observation in VGLUT1-expressing PC12 cells (Preobraschenski et al., 2018). To see whether VGLUTs can also use

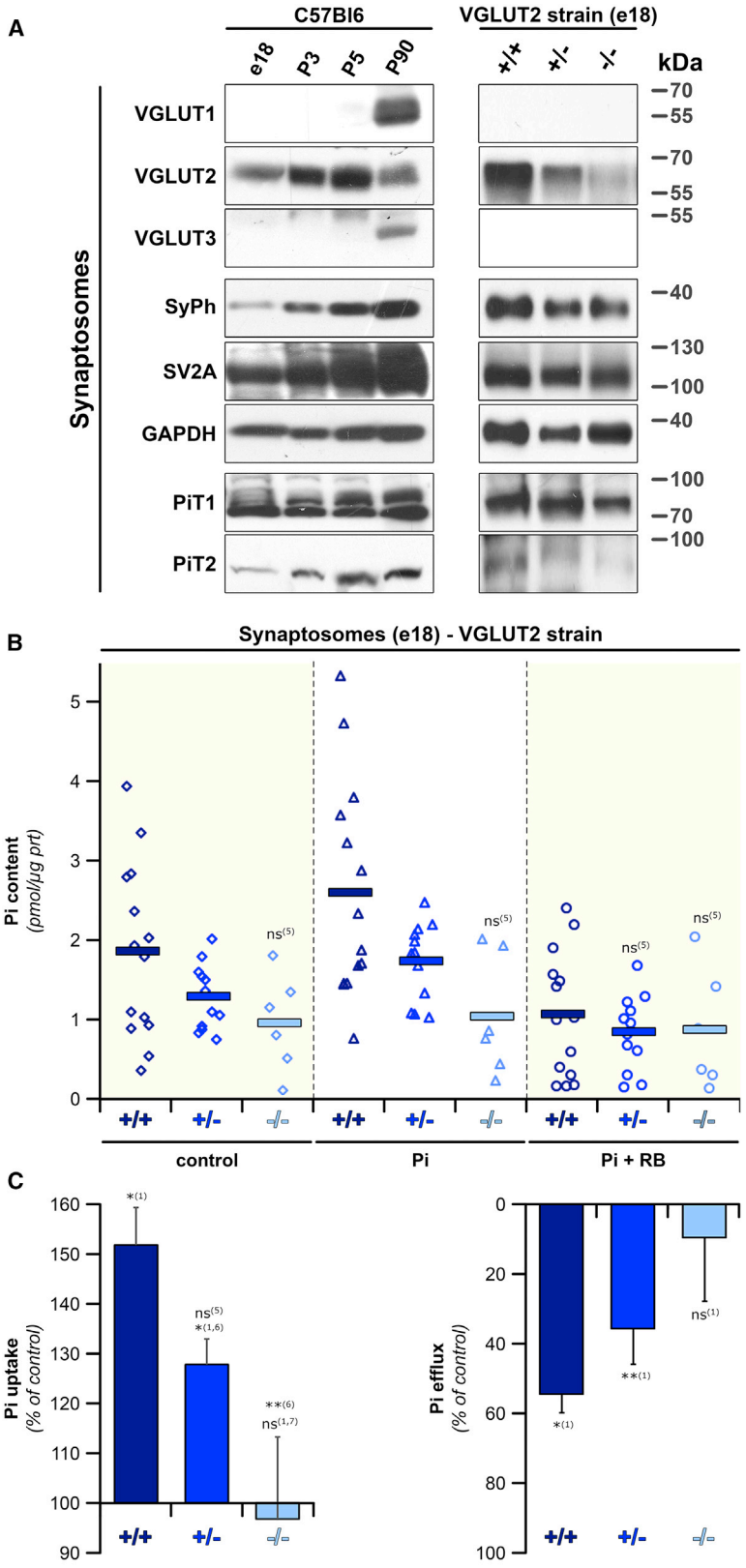

Figure 2. VGLUT2 Is a Key Factor of Synaptic [Pi] Homeostasis during Development

(A) Immunoblots (representative of 3–5 mice) show the expression of VGLUT1–3, synaptophysin (SyPh) and SV2A, GAPDH, and NaPi transporters PiT1 and 2 in murine synaptosomal preparations from developing (E18, postnatal day 3 [P3], and P5) or adult (P90) wild-type mice (left) or from E18 genotypes of the VGLUT2 mouse strains (right).

(B) Pi content of E18 synaptosomes obtained from the VGLUT2$^{-/-}$ strain was drastically reduced in the absence of VGLUTs.

(C) (Left) Normalized data from the experiments displayed in (B) show a genotype-specific decline of Pi uptake. (Right) Normalized data from (B) present the RB-mediated decrease in cytosolic Pi for each genotype as % of the control condition. In the absence of Pi, VGLUT activity restores Pi loss, a process inhibited by RB. No restoration of lost Pi takes place in the absence of any VGLUT, and RB has no effect.

Values represent pmol [Pi]/µg of protein for each genotype (B) or % of the control condition (no Pi offered; C). Data are the mean ± SEM from at least 6 mice per genotype. Significance toward: (1) no Pi added; (5) VGLUT2 KO control; (6) VGLUT2 WT; and (7) VGLUT2 Het.

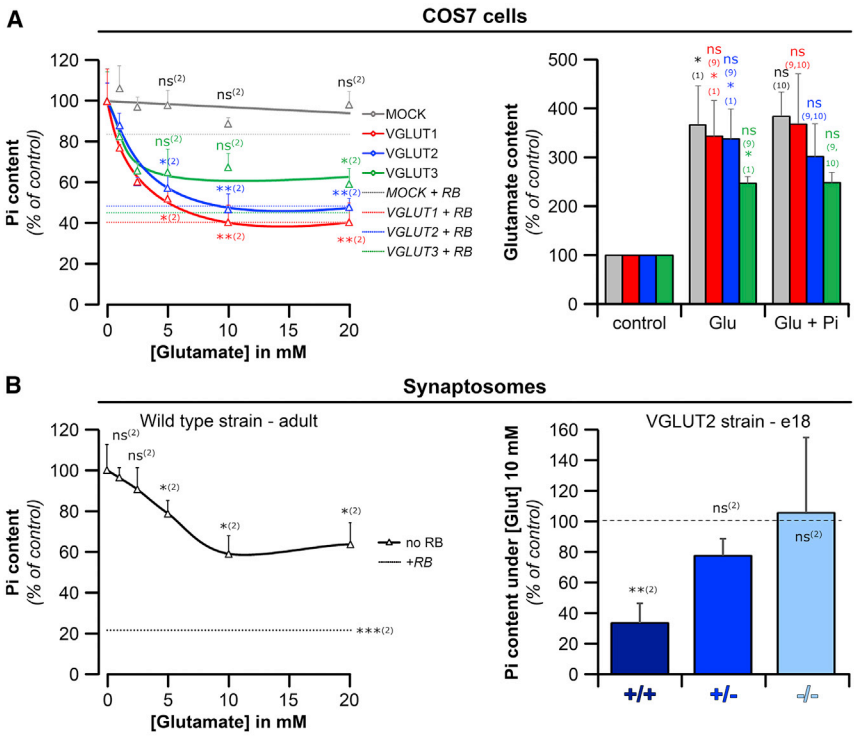

Figure 3. Glutamate Interferes with Pi Uptake by VGLUTs

(A) (Left) The Pi content of VGLUT-expressing COS7 cell lines was determined as in Figure 1. The cells were incubated in Pi-containing uptake buffer (10 mM) in the presence of increasing glutamate concentrations. (Right) In parallel experiments, glutamate content was measured after starving the cells in glutamate-free KREBS 4.7 mM [K^+] and then incubating them in uptake buffer ± 10 mM [Glu] ± 10 mM [Pi]. Note that all cell lines showed 2.5- to 4-fold higher glutamate content when incubated in 10 mM glutamate compared to cells receiving no glutamate (control). Glutamate uptake was not inhibited by 10 mM [Pi] (right Glu + Pi). In addition, it was not significantly changed by the expression of VGLUTs (Figure S3). The line colors given to the COS7-VGLUT cell lines (left panel) also apply to the bars (right panel).

(B) Pi uptake by synaptosomes prepared from adult rats (left) or from E18 mice of the VGLUT2 strains (right) after incubation with 10 mM [Pi] in the presence of increasing concentrations of glutamate. Inhibition saturated around 10 mM glutamate. In E18 synaptosomes, the extent of inhibition of Pi uptake by 10 mM glutamate (bars) correlated with VGLUT expression.

Data are shown as % of control (samples incubated with 10 mM [Pi] uptake buffer without glutamate, A, left and B, or glutamate and Pi-free buffer, A, right). Dotted lines in the left panels represent the condition Pi + RB and show the effect of complete VGLUT inhibition. Values represent the mean ± SEM from at least 3 independent experiments/animals (A and B). Significance toward: (1) no glutamate added; (2) Pi; (9) MOCK; and (10) glutamate.

glutamate under these conditions, we measured intracellular glutamate using the iGluSnFR sensor (Marvin et al., 2018) in control and VGLUT-expressing COS7 cell lines, applying a protocol of glutamate starvation followed by glutamate addition as for Pi measurements. All our COS7 cell lines accumulated glutamate when offered, irrespective of the presence of VGLUTs; Pi (10 mM) did not affect accumulation (Figure 3A, right). Resting glutamate levels did not depend on the absence or presence of VGLUTs (Figure S3B). Thus, VGLUTs in plasma membrane orientation are unable to import glutamate, confirming our previous observations (Preobraschenski et al., 2018).

Comparably, Pi uptake by synaptosomes was inhibited by glutamate (apparent Ki: 2.54 mM glutamate; Figure 3B, left). No such inhibition was seen when we carried out the same experiments using synaptosomes isolated from embryonal (E18) brain of VGLUT2$^{-/-}$ mice although synaptosomes from WT and heterozygous littermates were strongly or moderately inhibited, respectively (Figure 3B, right). Although glutamate inhibition of VGLUT-mediated Pi uptake is probably not physiologically relevant, the data further confirm that VGLUT-mediated Pi uptake plays a major role in keeping presynaptic Pi balance.

Using a VGLUT1-specific nanobody known to inhibit $\Delta\mu H^+$-driven glutamate uptake (Preobraschenski et al., 2018; Schenck et al., 2017), we aimed to clarify whether and how the conformational changes associated with glutamate translocation are connected to NaPi transport at the plasma membrane. To address this, we transfected COS7-VGLUT1 cells with a construct coding for the anti-VGLUT1 nanobody NB9 (Schenck et al., 2017) fused to mCherry under the control of a doxycycline-inducible TetOn promoter. Without induction, no expression of mCherry was detectable in either the TetOn:mCherry-NB9 or the TetOn:MOCK (Luciferase) COS7-VGLUT1 cells serving as control (Figure 4A). Overnight incubation with 500 ng/mL [doxycycline] initiated a massive expression of the mCherry-NB9 construct in the TetOn:mCherry-NB9 nanobody cells, whereas no expression occurred in the MOCK transfected control cells (Figure 4A). Expression of mCherry-NB9 strongly inhibited Pi uptake in the VGLUT1-expressing cells, comparable to the VGLUT inhibitor RB (Figure 4B). The absence of additive effect of NB9 and RB emphasizes the specificity of both inhibitors toward VGLUT1. Similar though less-pronounced results were obtained in cells expressing a fusion construct with swapped positions of NB9 and mCherry (COS7-VGLUT1-TetOn:NB9-mCherry; Figure S4).

We conclude that Pi uptake by VGLUT in the plasma membrane orientation involves conformational changes that are also required for glutamate uptake in the cytoplasmic orientation, emphasizing the link between these two transport modes. We assume that the nanobody, and perhaps some of the VGLUT inhibitors, prevent the switching between outward open/inward closed to inward open/outward closed conformation required for transport.

DISCUSSION

All VGLUTs have a major role in neuronal Pi homeostasis and therefore may be relevant to the vast majority of neurons in the CNS. Apparently, a dynamic balance between Pi import and efflux determines intracellular Pi levels, with VGLUTs making a significant contribution to uptake. Pi and glutamate may use

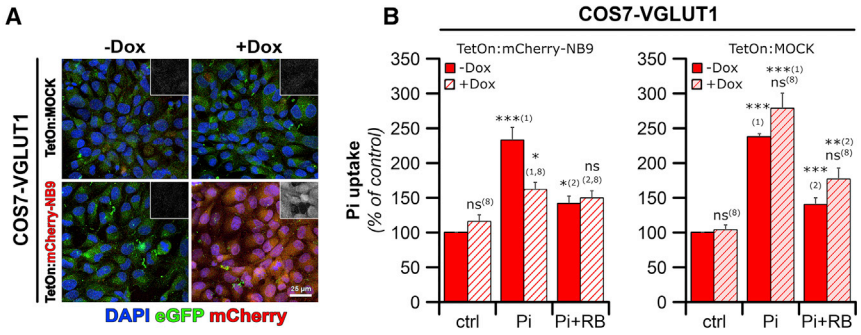

Figure 4. The VGLUT1-Specific NB9 Nanobody Abolishes Pi Transport by COS7-VGLUT1 Cells

(A) TetOn:mCherry-2A-NB9 expression was induced in COS7-VGLUT1-TetOn cells by overnight treatment with 500 ng/mL [doxycycline]. COS7-VGLUT1 cells transfected with a TetOn:luciferase construct served as MOCK control. EGFP and mCherry fluorescence signals were directly monitored by confocal microscopy as markers of VGLUT1 or NB9 expression, respectively. Scale bar, 25 μm.

(B) Pi content in COS7-VGLUT1-TetOn:mCherry-NB9 (left) or COS7-VGLUT1-TetOn:Luc (right) cells, preincubated in the absence (plain bars) or presence (striped bars) of doxycycline, shows that doxycycline-induced expression of NB9 reduced Pi uptake to levels comparable to those observed in the presence of RB (left). No effect of doxycycline was observed in the COS7-VGLUT1-TetOn:MOCK cell line (right).

All values are normalized to control (no doxycycline; no Pi) and represent mean values ± SEM from 4–13 experiments. Significance toward: (1) no Pi added; (2) Pi; and (8) no Dox.

overlapping binding sites for bidirectional transport, with inhibitory drugs and an inhibitory nanobody blocking both transport modes. During synaptic activity, VGLUTs shuttle between SVs and the plasma membrane, thereby linking neuronal activity to the recovery of presynaptic Pi stores.

VGLUTs are bifunctional transporters that physiologically transport Pi and glutamate in opposite directions, with each transport activity fueled by a different ion gradient (Preobraschenski et al., 2018) resembling other members of the SLC17A Pi transporter subfamily (Jutabha et al., 2010; Reimer, 2013; Togawa et al., 2012, 2015). Glutamate appears not to be an alternative substrate for Na^+-dependent import because cellular glutamate levels were not affected by additional expression of VGLUTs, confirming our earlier data (Preobraschenski et al., 2018) and supported by the structure (Li et al., 2020).

Besides the SLC17A family of Pi transporters, two other families of secondary active NaPi transporters are known, the SLC34 (NaPi IIa,b,c) and the SLC20 (PiT1 and PiT2) transporters (Forster et al., 2012). PiT1 and PiT2 are expressed in brain and considered to be the main transporters for Pi import by neurons and astrocytes (Chande and Bergwitz, 2018; Inden et al., 2016). In contrast, the mechanisms of Pi efflux are rather obscure. Imbalance between uptake and efflux is thought to cause severe pathological calcification of various tissues, including brain (Chande and Bergwitz, 2018; Giovannini et al., 2013; Yao et al., 2017; Zhang et al., 2014). In our experiments with synaptosomes a considerable Pi efflux is counteracted by VGLUT activity, the underlying mechanism remains to be resolved.

Surprisingly little is known about Pi homeostasis in neurons and in presynaptic nerve terminals. Besides cellular import and export, Pi levels are modulated by mitochondria and by enzymatic conversion, most importantly during synthesis and breakdown of nucleotides and polyphosphates (Chande and Bergwitz, 2018). Remarkably, Pi uptake capacity of neurons increases upon stimulation of exocytosis, suggesting a tight coupling between synaptic activity and Pi homeostasis. Presumably, the high energy demand of synaptic vesicle recycling and vesicle reloading with transmitter results in major Pi fluctuations, although it is not clear whether synaptic activity is directly linked to Pi loss from the cytoplasm. Because VGLUTs are integrated transiently into the plasma membrane during exocytosis (Balaji and Ryan, 2007), Pi uptake is transiently increased. Thus, SVs constitute a reservoir for Pi-transporting VGLUTs at the plasma membrane comparable to other "reserve" transporter transiently inserted into the plasma membrane, like GLUT4 vesicles to recover glucose (Ashrafi et al., 2017) or GABA transporter vesicles to regain released GABA (Deken et al., 2003). However, VGLUTs represent unusual examples of a "transporter reservoir" in which the transporter uses completely different transport modes in the vesicle and at the plasma membrane.

Intriguingly, several lines of evidence suggest that re-endocytosis of VGLUTs following SV exocytosis involves unusual pathways using endophilin, intersectin (Richter et al., 2018; Voglmaier et al., 2006), or AP-1 and AP-3 (Li et al., 2017). It is thus conceivable that VGLUTs' residence in the presynaptic plasma membrane is regulated differently from the bulk of synaptic vesicle proteins. Indeed, we have shown earlier that VGLUT1 and VGLUT2 selectively shift to the plasma membrane controlled by circadian regulation (Darna et al., 2009; Yelamanchili et al., 2006).

Much is still to be learned about the intracellular balance of Pi, involved in a myriad of metabolic processes. In particular, the functional interplay between VGLUTs and the canonical Pi transporters PiT1 and PiT2 remains to be resolved. Although both PiTs are present in VGLUT2$^{-/-}$ synaptosomes, they cannot compensate for the lack of VGLUTs to correct Pi cytosolic homeostasis. Similarly, though PiT2 expression was decreased in VGLUT2$^{-/-}$ synaptosomes (Figure 3A, right), VGLUT inhibitor RB failed to reduce VGLUT2$^{-/-}$ synaptosomal Pi levels any further, clearly indicating that VGLUTs play a role in the Pi balance. PiTs, distributed abundantly, maintain basic Pi balance, and may also regulate Pi homeostasis in neurons not expressing any VGLUT.

Taken together, the Pi balance between the cytoplasm and the extracellular space at synaptic terminals is maintained by two activities, VGLUTs undertaking Pi import and an observed efflux, the nature of which is still unclear. The expression of VGLUTs in glutamatergic and non-glutamatergic neurons and their function as Pi transporters is linked to synaptic Pi homeostasis, although the physiological input needs to be more specified.

STAR★METHODS

Detailed methods are provided in the online version of this paper and include the following:

- KEY RESOURCES TABLE
- RESOURCE AVAILABILITY
  - Lead Contact
  - Materials Availability
  - Data and Code Availability
- EXPERIMENTAL MODEL AND SUBJECT DETAILS
  - Cell culture models
  - Synaptosomes
- METHOD DETAILS
  - Pi measurement in cells and synaptosomes
  - Glutamate uptake
  - Immunofluorescence microscopy and immunoblots
  - Dilution of Antibodies
  - Image treatment
- QUANTIFICATION AND STATISTICAL ANALYSIS

SUPPLEMENTAL INFORMATION

Supplemental Information can be found online at https://doi.org/10.1016/j.celrep.2020.108623.

ACKNOWLEDGMENTS

We acknowledge the excellent technical support provided by Marion Moebes, Birgit Metze, Antje Dräger (Institute for Integrative Neuroanatomie, Berlin), and Brigitte Barg-Kues (Max-Planck-Institute for Biophysical Chemistry, Göttingen). We also thank Dr. Thorsten Trimbuch for the gift of VGLUT2$^{-/-}$ mice. Work was supported by grants to G.A.-H. and R.J. from the Deutsche Forschungsgemeinschaft ('AH67/7-2 and JA 377/6-2) and by an ERC Advanced Grant (SVNeuroTrans) to R.J.

AUTHOR CONTRIBUTIONS

C.C., R.J., and G.A.-H. planned the study and wrote the manuscript. C.C., M.G., and J.P. performed the experiments.

DECLARATION OF INTERESTS

The authors declare no competing interests.

Received: May 11, 2020
Revised: September 28, 2020
Accepted: December 17, 2020
Published: January 12, 2021

REFERENCES

Aihara, Y., Mashima, H., Onda, H., Hisano, S., Kasuya, H., Hori, T., Yamada, S., Tomura, H., Yamada, Y., Inoue, I., et al. (2000). Molecular cloning of a novel brain-type Na(+)-dependent inorganic phosphate cotransporter. J. Neurochem. *74*, 2622–2625.

Anne, C., and Gasnier, B. (2014). Vesicular neurotransmitter transporters: mechanistic aspects. Curr. Top. Membr. *73*, 149–174.

Ashrafi, G., Wu, Z., Farrell, R.J., and Ryan, T.A. (2017). GLUT4 mobilization supports energetic demands of active synapses. Neuron *93*, 606–615.e3.

Balaji, J., and Ryan, T.A. (2007). Single-vesicle imaging reveals that synaptic vesicle exocytosis and endocytosis are coupled by a single stochastic mode. Proc. Natl. Acad. Sci. USA *104*, 20576–20581.

Becher, A., Drenckhahn, A., Pahner, I., Margittai, M., Jahn, R., and Ahnert-Hilger, G. (1999). The synaptophysin-synaptobrevin complex: a hallmark of synaptic vesicle maturation. J. Neurosci. *19*, 1922–1931.

Bellocchio, E.E., Reimer, R.J., Fremeau, R.T., Jr., and Edwards, R.H. (2000). Uptake of glutamate into synaptic vesicles by an inorganic phosphate transporter. Science *289*, 957–960.

Boulland, J.L., Qureshi, T., Seal, R.P., Rafiki, A., Gundersen, V., Bergersen, L.H., Fremeau, R.T., Jr., Edwards, R.H., Storm-Mathisen, J., and Chaudhry, F.A. (2004). Expression of the vesicular glutamate transporters during development indicates the widespread corelease of multiple neurotransmitters. J. Comp. Neurol. *480*, 264–280.

Chande, S., and Bergwitz, C. (2018). Role of phosphate sensing in bone and mineral metabolism. Nat. Rev. Endocrinol. *14*, 637–655.

Darna, M., Schmutz, I., Richter, K., Yelamanchili, S.V., Pendyala, G., Höltje, M., Albrecht, U., and Ahnert-Hilger, G. (2009). Time of day-dependent sorting of the vesicular glutamate transporter to the plasma membrane. J. Biol. Chem. *284*, 4300–4307.

Deken, S.L., Wang, D., and Quick, M.W. (2003). Plasma membrane GABA transporters reside on distinct vesicles and undergo rapid regulated recycling. J. Neurosci. *23*, 1563–1568.

Edwards, R.H. (2007). The neurotransmitter cycle and quantal size. Neuron *55*, 835–858.

El Mestikawy, S., Wallén-Mackenzie, A., Fortin, G.M., Descarries, L., and Trudeau, L.E. (2011). From glutamate co-release to vesicular synergy: vesicular glutamate transporters. Nat. Rev. Neurosci. *12*, 204–216.

Eriksen, J., Chang, R., McGregor, M., Silm, K., Suzuki, T., and Edwards, R.H. (2016). Protons regulate vesicular glutamate transporters through an allosteric mechanism. Neuron *90*, 768–780.

Forster, I.C., Hernando, N., Biber, J., and Murer, H. (2012). Phosphate transport kinetics and structure-function relationships of SLC34 and SLC20 proteins. Curr. Top. Membr. *70*, 313–356.

Giovannini, D., Touhami, J., Charnet, P., Sitbon, M., and Battini, J.L. (2013). Inorganic phosphate export by the retrovirus receptor XPR1 in metazoans. Cell Rep. *3*, 1866–1873.

Gras, C., Amilhon, B., Lepicard, E.M., Poirel, O., Vinatier, J., Herbin, M., Dumas, S., Tzavara, E.T., Wade, M.R., Nomikos, G.G., et al. (2008). The vesicular glutamate transporter VGLUT3 synergizes striatal acetylcholine tone. Nat. Neurosci. *11*, 292–300.

Grosse, G., Draguhn, A., Höhne, L., Tapp, R., Veh, R.W., and Ahnert-Hilger, G. (2000). Expression of Kv1 potassium channels in mouse hippocampal primary cultures: development and activity-dependent regulation. J. Neurosci. *20*, 1869–1882.

Hayashi, M., Otsuka, M., Morimoto, R., Hirota, S., Yatsushiro, S., Takeda, J., Yamamoto, A., and Moriyama, Y. (2001). Differentiation-associated Na+-dependent inorganic phosphate cotransporter (DNPI) is a vesicular glutamate transporter in endocrine glutamatergic systems. J. Biol. Chem. *276*, 43400–43406.

Inden, M., Iriyama, M., Zennami, M., Sekine, S.I., Hara, A., Yamada, M., and Hozumi, I. (2016). The type III transporters (PiT-1 and PiT-2) are the major sodium-dependent phosphate transporters in the mice and human brains. Brain Res. *1637*, 128–136.

Juge, N., Yoshida, Y., Yatsushiro, S., Omote, H., and Moriyama, Y. (2006). Vesicular glutamate transporter contains two independent transport machineries. J. Biol. Chem. *281*, 39499–39506.

Juge, N., Gray, J.A., Omote, H., Miyaji, T., Inoue, T., Hara, C., Uneyama, H., Edwards, R.H., Nicoll, R.A., and Moriyama, Y. (2010). Metabolic control of vesicular glutamate transport and release. Neuron *68*, 99–112.

Jutabha, P., Anzai, N., Kitamura, K., Taniguchi, A., Kaneko, S., Yan, K., Yamada, H., Shimada, H., Kimura, T., Katada, T., et al. (2010). Human sodium phosphate transporter 4 (hNPT4/SLC17A3) as a common renal secretory pathway for drugs and urate. J. Biol. Chem. *285*, 35123–35132.

Li, H., Santos, M.S., Park, C.K., Dobry, Y., and Voglmaier, S.M. (2017). VGLUT2 trafficking is differentially regulated by adaptor proteins AP-1 and AP-3. Front. Cell. Neurosci. *11*, 324.

Li, F., Eriksen, J., Finer-Moore, J., Chang, R., Nguyen, P., Bowen, A., Myasnikov, A., Yu, Z., Bulkley, D., Cheng, Y., et al. (2020). Ion transport and regulation in a synaptic vesicle glutamate transporter. Science *368*, 893–897.

Marazzi, G., and Buckley, K.M. (1993). Accumulation of mRNAs encoding synaptic vesicle-specific proteins precedes neurite extension during early neuronal development. Dev. Dyn. *197*, 115–124.

Martineau, M., Guzman, R.E., Fahlke, C., and Klingauf, J. (2017). VGLUT1 functions as a glutamate/proton exchanger with chloride channel activity in hippocampal glutamatergic synapses. Nat. Commun. *8*, 2279.

Marvin, J.S., Scholl, B., Wilson, D.E., Podgorski, K., Kazemipour, A., Müller, J.A., Schoch, S., Quiroz, F.J.U., Rebola, N., Bao, H., et al. (2018). Stability, affinity, and chromatic variants of the glutamate sensor iGluSnFR. Nat. Methods *15*, 936–939.

Moechars, D., Weston, M.C., Leo, S., Callaerts-Vegh, Z., Goris, I., Daneels, G., Buist, A., Cik, M., van der Spek, P., Kass, S., et al. (2006). Vesicular glutamate transporter VGLUT2 expression levels control quantal size and neuropathic pain. J. Neurosci. *26*, 12055–12066.

Münster-Wandowski, A., Zander, J.F., Richter, K., and Ahnert-Hilger, G. (2016). Co-existence of functionally different vesicular neurotransmitter transporters. Front. Synaptic Neurosci. *8*, 4.

Nakamura, N., Tanaka, S., Teko, Y., Mitsui, K., and Kanazawa, H. (2005). Four Na+/H+ exchanger isoforms are distributed to Golgi and post-Golgi compartments and are involved in organelle pH regulation. J. Biol. Chem. *280*, 1561–1572.

Ni, B., Rosteck, P.R., Jr., Nadi, N.S., and Paul, S.M. (1994). Cloning and expression of a cDNA encoding a brain-specific Na(+)-dependent inorganic phosphate cotransporter. Proc. Natl. Acad. Sci. USA *91*, 5607–5611.

Preobraschenski, J., Zander, J.F., Suzuki, T., Ahnert-Hilger, G., and Jahn, R. (2014). Vesicular glutamate transporters use flexible anion and cation binding sites for efficient accumulation of neurotransmitter. Neuron *84*, 1287–1301.

Preobraschenski, J., Cheret, C., Ganzella, M., Zander, J.F., Richter, K., Schenck, S., Jahn, R., and Ahnert-Hilger, G. (2018). Dual and direction-selective mechanisms of phosphate transport by the vesicular glutamate transporter. Cell Rep. *23*, 535–545.

Reimer, R.J. (2013). SLC17: a functionally diverse family of organic anion transporters. Mol. Aspects Med. *34*, 350–359.

Reimer, R.J., and Edwards, R.H. (2004). Organic anion transport is the primary function of the SLC17/type I phosphate transporter family. Pflugers Arch. *447*, 629–635.

Richter, K., Schmutz, I., Darna, M., Zander, J.F., Chavan, R., Albrecht, U., and Ahnert-Hilger, G. (2018). VGLUT1 binding to endophilin or intersectin1 and dynamin phosphorylation in a diurnal context. Neuroscience *371*, 29–37.

Schenck, S., Kunz, L., Sahlender, D., Pardon, E., Geertsma, E.R., Savtchouk, I., Suzuki, T., Neldner, Y., Štefanić, S., Steyaert, J., et al. (2017). Generation and characterization of anti-VGLUT nanobodies acting as inhibitors of transport. Biochemistry *56*, 3962–3971.

Seal, R.P., Akil, O., Yi, E., Weber, C.M., Grant, L., Yoo, J., Clause, A., Kandler, K., Noebels, J.L., Glowatzki, E., et al. (2008). Sensorineural deafness and seizures in mice lacking vesicular glutamate transporter 3. Neuron *57*, 263–275.

Takamori, S., Rhee, J.S., Rosenmund, C., and Jahn, R. (2000). Identification of a vesicular glutamate transporter that defines a glutamatergic phenotype in neurons. Nature *407*, 189–194.

Takamori, S., Rhee, J.S., Rosenmund, C., and Jahn, R. (2001). Identification of differentiation-associated brain-specific phosphate transporter as a second vesicular glutamate transporter (VGLUT2). J. Neurosci. *21*, RC182.

Takamori, S., Malherbe, P., Broger, C., and Jahn, R. (2002). Molecular cloning and functional characterization of human vesicular glutamate transporter 3. EMBO Rep. *3*, 798–803.

Togawa, N., Miyaji, T., Izawa, S., Omote, H., and Moriyama, Y. (2012). A Na+-phosphate cotransporter homologue (SLC17A4 protein) is an intestinal organic anion exporter. Am. J. Physiol. Cell Physiol. *302*, C1652–C1660.

Togawa, N., Juge, N., Miyaji, T., Hiasa, M., Omote, H., and Moriyama, Y. (2015). Wide expression of type I Na+-phosphate cotransporter 3 (NPT3/SLC17A2), a membrane potential-driven organic anion transporter. Am. J. Physiol. Cell Physiol. *309*, C71–C80.

Voglmaier, S.M., Kam, K., Yang, H., Fortin, D.L., Hua, Z., Nicoll, R.A., and Edwards, R.H. (2006). Distinct endocytic pathways control the rate and extent of synaptic vesicle protein recycling. Neuron *51*, 71–84.

Wallén-Mackenzie, A., Gezelius, H., Thoby-Brisson, M., Nygård, A., Enjin, A., Fujiyama, F., Fortin, G., and Kullander, K. (2006). Vesicular glutamate transporter 2 is required for central respiratory rhythm generation but not for locomotor central pattern generation. J. Neurosci. *26*, 12294–12307.

Wojcik, S.M., Rhee, J.S., Herzog, E., Sigler, A., Jahn, R., Takamori, S., Brose, N., and Rosenmund, C. (2004). An essential role for vesicular glutamate transporter 1 (VGLUT1) in postnatal development and control of quantal size. Proc. Natl. Acad. Sci. USA *101*, 7158–7163.

Yao, X.P., Zhao, M., Wang, C., Guo, X.X., Su, H.Z., Dong, E.L., Chen, H.T., Lai, J.H., Liu, Y.B., Wang, N., and Chen, W.J. (2017). Analysis of gene expression and functional characterization of XPR1: a pathogenic gene for primary familial brain calcification. Cell Tissue Res. *370*, 267–273.

Yelamanchili, S.V., Pendyala, G., Brunk, I., Darna, M., Albrecht, U., and Ahnert-Hilger, G. (2006). Differential sorting of the vesicular glutamate transporter 1 into a defined vesicular pool is regulated by light signaling involving the clock gene Period2. J. Biol. Chem. *281*, 15671–15679.

Zhang, Y., Chen, K., Sloan, S.A., Bennett, M.L., Scholze, A.R., O'Keeffe, S., Phatnani, H.P., Guarnieri, P., Caneda, C., Ruderisch, N., et al. (2014). An RNA-sequencing transcriptome and splicing database of glia, neurons, and vascular cells of the cerebral cortex. J. Neurosci. *34*, 11929–11947.

STAR★METHODS

KEY RESOURCES TABLE

REAGENT or RESOURCE	SOURCE	IDENTIFIER
Antibodies		
Rat eGFP	Nacalai Tesque	04404-84
Guinea pig VGLUT1 (SLC17A7)	Synaptic Systems	135304
Rabbit VGLUT1 (SLC17A7)	Synaptic Systems	135302
Guinea pig VGLUT2 (SLC17A6)	Synaptic Systems	135404
Rabbit VGLUT2 (SLC17A6)	Synaptic Systems	135402
Rabbit VGLUT3 (SLC17A8)	Synaptic Systems	135203
Mouse Synaptophysin	Synaptic Systems	101011
Rabbit SV2A	Synaptic Systems	119003
Mouse GAPDH	Millipore	MAB374
Rabbit PiT1 (SLC20A1)	Gene Tex	GTX64727
Mouse PiT2 (SLC20A2)	Santa Cruz Biotech.	sc-377326
Goat anti-Rat Alexa 488	Abcam	ab150157
Goat anti-Guinea pig Alexa 555	Abcam	ab150186
Donkey anti-Rabbit Cy5	Jackson Immunoresearch	711-175-152
Goat anti-Rabbit HRP	Vector	PI-1000
Horse anti-Mouse HRP	Vector	PI-2000
Guinea pig anti-Mouse (light chain) HRP	Dianova	115-035-174
Bacterial and Virus Strains		
DH10B	Institute for Integrative Neuroanatomy	N/A
Stellar *E. coli*	Takara, Nojihigashi Japan	636766
Biological Samples		
Synaptosome preparations C57Bl6j	Institute for Integrative Neuroanatomy	N/A
Synaptosome preparations VGLUT2^{NULL} mouse strain	Institute for Integrative Neuroanatomy	N/A
Synaptosome preparations Wistar Rats	Institute for Integrative Neuroanatomy	N/A
Chemicals, Peptides, and Recombinant Proteins		
Immumount	ThermoFisher Scientific, Waltham USA	#10662815
iGluSnFR A184S	kindly provided by L. Looger, (HHMI, Janelia Research Campus USA)	N/A
Lipofectamin 2000	ThermoFisher Scientific, Waltham USA	# 11668019
Opti-MEM I	GIBCO/BRL Life Technologies Eggenstein, Germany.	11058021
Fetal Bovine Serum	Sigma	S0615
Horse Serum	GIBCO	16050-122
Bovine Serum Albumin	Roth	T844.4
media supplemented with 1% L-glutamine and penicillin/ streptomycin	GIBCO/BRL Life Technologies Eggenstein, Germany.	35050038
Dynasore	Sigma	D7693-5MG
Glycine	Roth	3908.2
NaGluconate	Sigma	S2054
NaGlutamate	Sigma	G-1626
NaCl	Roth	3957.1
NaH_2PO_4	Merck	1.06346.0500
Na_2HPO_4	Roth	P030.1
KCl	Merck	4936.0500
KH_2PO_4	Fluka	60230

(*Continued on next page*)

Continued

REAGENT or RESOURCE	SOURCE	IDENTIFIER
K_2HPO_4	Fluka	60355
$MgSO_4$	Merck	1.05886.0500
$CaCl_2$	Roth	5239.1
HEPES	Sigma	H3375-250G
Glucose	Roth	HN06.2
Evans Blue	Aldrich	E2125-10G
Rose Bengale	Aldrich	330000-1G
Critical Commercial Assays		
Malachite green/molybdate assay	Biomol green, BML	BML-AK111
ECL detection system	GE Healthcare, Munich Germany	GERPN2209
Tet System Approved FBS	Takara, Nojihigashi Japan	#631106 FBS*
pTetOne backbone inFusion system	Takara, Nojihigashi Japan	#634301/638916
Deposited Data		
STAR*Dataset	Institute for Integrative Neuroanatomy	N/A
Experimental Models: Cell Lines		
COS7-VGLUT1,2,3 or MOCK cell lines, multiple clones	Institute for Integrative Neuroanatomy	N/A
COS7-VGLUT1-TetOn-NB9-2A-mCherry cell line, 1 clone based on COS7-VGLUT1 clone 5	Institute for Integrative Neuroanatomy	N/A
COS7-VGLUT1-TetOn-mCherry-2A-NB9 cell line, multiple clones based on COS7-VGLUT1 clone 5	Institute for Integrative Neuroanatomy	N/A
COS7-VGLUT1-TetOn-Luciferase cell line, 1 clone based on COS7-VGLUT1 clone 5	Institute for Integrative Neuroanatomy	N/A
HEK293A-VGLUT1,2,3 or MOCK cell lines, multiple clones	Institute for Integrative Neuroanatomy	N/A
PC12-VGLUT1,2 or MOCK cell lines, multiple clones	Lutz Birnbaumer (BIOMED), Catholic University Buenos Aires, Argentina	N/A
Experimental Models: Organisms/Strains		
RjOrl:Swiss mice	Janvier Saint Berthevin France)	N/A
adult RjHan:Wi rats	Janvier Saint Berthevin France)	N/A
adult C57Bl6 mice (C57Bl6)	Janvier Saint Berthevin France)	N/A
$VGLUT2^{NULL}$ mouse strain	Christian Rosenmund's lab, Institute for Neurophysiology, Charité Berlin, Germany)	N/A
Recombinant DNA		
pcDNA4-anti-VGLUT1 nanobody NB9	Schenck et al., 2017	N/A
Plasmid: pcDNA3-rVGLUT1, G418 resistance, multiple clones	Institute for Integrative Neuroanatomy	N/A
Plasmid: pcDNA3-rVGLUT2, G418 resistance, multiple clones	Institute for Integrative Neuroanatomy	N/A
Plasmid: pcDNA3-rVGLUT3, G418 resistance, multiple clones	Institute for Integrative Neuroanatomy	N/A
Plasmid: pC1-eGFP, G418 resistance, multiple clones Used as MOCK in COS7 and HEK293A experiments	Institute for Integrative Neuroanatomy	N/A
Plasmid: pTetOne-NB9-2A-mCherry, no eukaryotic resistance (brought by cotransfection, Takara infusion protocol), multiple clones	Institute for Integrative Neuroanatomy	N/A
Plasmid: pTetOne-mCherry −2A-NB9, no eukaryotic resistance (brought by cotransfection, Takara infusion protocol), multiple clones	Institute for Integrative Neuroanatomy	N/A
Plasmid: pTetOne-Luc, no eukaryotic resistance (brought by cotransfection, Takara infusion protocol), multiple clones	Takara, Nojihigashi Japan	638918

RESOURCE AVAILABILITY

Lead Contact

Further information and requests for resources and reagents should be directed to and will be fulfilled by the Lead Contact Gudrun Ahnert-Hilger (gahnert@gwdg.de)

Materials Availability

No new materials were generated for this study, and all materials are commercially available. The new vectors and cell lines generated during the course of the study are available on request.

Data and Code Availability

Datasets will be made available upon reasonable request.

EXPERIMENTAL MODEL AND SUBJECT DETAILS

Cell culture models

PC12 cell lines stably expressing either murine VGLUT1, VGLUT2 or an empty vector (MOCK) (kindly provided by Lutz Birnbaumer (BIOMED), Catholic University Buenos Aires, Argentina) were cultivated in DMEM/FBS/HS (fetal bovine serum/horse serum) 85/5/10 + 800 μg/mL [geneticin] (G418), under 10% CO_2 at 37°C.

COS7 and HEK293A cells were transfected with pcDNA3.1 vectors containing VGLUT-IRES-eGFP constructs specific for VGLUT1 (rat), VGLUT2 or VGLUT3 (both human) coding data sequences and a G418 resistance gene. A pC1-eGFP vector with similar resistance served as control (MOCK). GFP-expressing cells were selected by the application of 400 μg/mL [G418], followed by FACS. From each selected and FAC-sorted transfection pool, clones were obtained by extreme dilution and kept under G418 selection (400 μg/mL). Cells displaying similar, physiological growth rates were chosen for further experiments. All related clones (specific for either VGLUT-1, −2, −3 or MOCK) showed comparable Pi uptake properties, respectively. COS7 cells were grown in DMEM/FBS 90/10 + 400 μg/mL [G418], while HEK293A cells were grown in Eagle's medium/FBS 95/5 + 400 μg/mL [G418], both under 5% CO_2 at 37°C.

For the experiments involving co-expression of a nanobody specific for VGLUT1, the COS7-VGLUT1 clone used for Pi uptake experiments was further modified. To ensure minimal baseline induction, cells were cultivated using Tet System Approved FBS (FBS*). VGLUT1-specific nanobody NB9 constructs (kindly provided by S. Schenck and R. Dutzler, Zürich, described in Schenck et al. (2017) were coupled with a 2A linker to mCherry and then sub-cloned into a doxycycline-inducible pTetOne backbone using the inFusion system. Inducible vectors containing NB9-mCherry in either orientation (N-terminal NB9 or N-terminal mCherry) were thus obtained and vector clones (4 mCherry-NB9, 1 NB9-mCherry, 1 unmodified pTetOne-Luc containing luciferase as MOCK) were used to transfect COS7-VGLUT1 cells along with a puromycin resistance sequence to establish stable cell lines as described by the provider. Transfected cells were then treated overnight with 500 ng/mL doxycycline, and $eGFP^+$/$mCherry^+$ expressing cells from each cell line were selected by FACS and further cultivated and maintained in DMEM/FBS* 90/10 + 400 μg/mL [G418] + 250 ng/mL [puromycin] under 5% CO_2 at 37°C. Following FACS, cells were cultivated in such doxycycline-free medium for at least seven days to allow the doxycycline-induced NB9 expression to recess (checked by immunofluorescence) before performing Pi uptake experiments. For Pi uptake experiments, NB9 expression was induced in half of the wells seeded with COS7-VGLUT1-TetOn cells by overnight incubation with 500 ng/mL [doxycycline], the other half was used as control.

Primary neuronal cultures were obtained from fetal (e16) Swiss mice and cultivated as mixed hippocampal/cortical cultures as described previously (Grosse et al., 2000). Neurons were seeded on a coat of poly-L-lysin/collagen in 24-well plates at 1.5×10^5 cells per well for measuring Pi-uptake.

All media were supplemented with 1% L-glutamine and penicillin/streptomycin.

Synaptosomes

For synaptosomal preparations adult Wistar rats (female 4-6 months) and mice (C57Bl6, femal 3-5 months) were kept until use under a 12/12 h light/dark cycle with food and water *ad libitum*. $VGLUT2^{-/-}$ (NULL allele, either sex) mice (Moechars et al., 2006) were kindly provided by T. Trimbuch and C. Rosenmund (Charité Berlin, Germany). P2 fractions (synaptosomes) from adult or fetal brains were isolated according to previous publications (Becher et al., 1999). Briefly, the forebrain from one animal was homogenized in a glass/Teflon potter system in 3.5 or 7 mL (e18 or adult, respectively) of 300 mM sucrose buffer, incubated 5 minutes with 2 μL RNase/DNase I V/V solution. This solution was then processed at 4°C for all following steps: cell debris (P1) were pelleted at 1,350 g and the supernatant containing synaptosomes (S1) further centrifuged at 14,000 g in order to obtain a synaptosome pellet (P2). The P2 preparation was then used for functional (Pi uptake/release) or biochemical (western blot) experiments.

The local Animal Welfare Act (LaGeSo Berlin T0119/11) issued certificate of approval for using animals.

METHOD DETAILS

Pi measurement in cells and synaptosomes

For all cell models, Pi uptake was performed with cultures at 70%–80% cell density. To measure the proportion of Pi uptake mediated by VGLUTs, the VGLUT-specific inhibitors Evans Blue (2 μM [EB], PC12 cells) or Rose Bengal (10 μM [RB], all other systems) were added, at concentrations shown to inhibit VGLUT activity to a comparable degree (Anne and Gasnier, 2014). Inhibitors were always added after the starvation, depolarization and repolarization steps.

Cultured primary neurons and PC12-VGLUT cell lines (see above) were starved for Pi in a modified KREBS Buffer (135.3 mM [Na^+] // 4.7 mM [K^+] // 140 mM [Cl^-] // 1 mM [$MgSO_4$] // 500 μM [$CaCl_2$] // 20 mM [HEPES] // 20 mM [Glucose]) pH 7.4 (KREBS 4.7 mM [K^+]) for 1 h prior to the experiment. Translocation of VGLUT from vesicular compartments to the plasma membrane was induced by exposing the cells to high [K^+] KREBS buffer (110 mM [Na^+] // 30 mM [K^+] // 140 mM [Cl^-] // 1 mM [$MgSO_4$] // 2.5 mM [$CaCl_2$] // 20 mM [HEPES] // 20 mM [Glucose]) pH 7.4 (KREBS 30 mM [K^+]) for 10 minutes. Cells were quickly washed and allowed to repolarize in KREBS 4.7 mM [K^+] for 30 min. Endocytosis was blocked by complementing all KREBS buffers with 80 μM [dynasore] to maximize VGLUT localization at the plasma membrane.

Cells were detached and quickly washed (10,000 g for 30 s at 4°C) twice with glycine buffer (240 mM [glycine], 20 mM [HEPES], 20 mM [glucose], pH 7.0). Uptake (15 min at 37°C) was initiated by adding a physiological salt solution (90 mM [NaCl], 60 mM [glycine], 20 mM [HEPES] and 20 mM [glucose] at pH 7.0 and up to 30 mM [NaGluconate] balanced to 340 mOs for all conditions), called "uptake buffer" thereafter. Depending on conditions used, all or part of the NaGluconate was replaced by 10 mM [NaPi] and/or 1-20 mM [NaGlutamate]. EB (2 μM) or RB (10 μM) were added for negative controls.

Following uptake incubation, the reaction was stopped by quickly transferring the samples on ice followed by two fast washing steps with ice-cold glycine buffer and centrifugation > 10,000 g for 30 s at 4°C. Cell pellets were then lysed in 250 μL sterile ice-cold water for 20 min while shaking at 1,000 rpm. Samples were transferred into ultracentrifugation tubes and centrifuged at 357,000 g for 10 min at 4°C. The Pi content in the supernatant (diluted cytosol) was determined using a malachite green/molybdate assay measuring the optical density at 620 nm. During the course of experiments, we found that in all models except PC12 cells (that do not retain this dye) EB visually interferes with malachite green-based Pi measurement. Thus, RB was preferred in experiments using COS7, HEK293A and synaptosomes for VGLUT inhibition. For quantification, the Pi content was normalized to the number of cells per data point.

Pi uptake into COS7 or HEK293A (VGLUT- or MOCK-transfected) was performed as described above except that the depolarization step (KREBS 30 mM [K^+]) was omitted and the Pi starvation period was extended to 2 hours.

Freshly prepared synaptosomes (P2) from either adult rat (4-6 months, female) or adult (3 months, female)/ postnatal (p3-p5)/ fetal (e18) mouse forebrains (either sex) prepared in sucrose buffer (300 mM), were depolarized by resuspension in KREBS 30 mM [K^+] followed by incubation for 15 minutes and finally spun down. Pelleted synaptosomes were incubated in KREBS 4.7 mM [K^+] for 25 min to allow for repolarization, then quickly washed twice in glycine buffer, and finally incubated in 340 mOs uptake buffers as described for PC12 cell lines. As above, all KREBS buffers contained 80 μM [dynasore] to prevent endocytosis of the VGLUTs. In these experiments, the Pi content was normalized to the amount of protein (5 and 1 mg proteins per mL for adult and e18 synaptosomes, respectively).

To study efflux of Pi, synaptosomes derived from adult brains were preloaded with Pi by incubation for 15 minutes in KREBS 30 mM [K^+] containing 10 mM [Pi] (for depolarization and Pi-loading). Synaptosomes were then pelleted, resuspended and incubated in KREBS 4.7 mM [K^+] supplemented with 10 mM [Pi] for 25 minutes to allow for repolarization and further Pi-loading. Synaptosomes were then quickly washed twice in glycine buffer and incubated in Pi-free uptake buffer in the presence or absence of RB for either 2 or 15 min at 37°C. Tubes were quickly transferred onto an ice slurry to stop ion transport, then centrifuged for 1 min at > 10,000 g at 4°C. Supernatants were taken to measure Pi content in the external milieu (released Pi), while pellets were washed twice with glycine buffer and osmotically lysed in ddH_2O under shaking as described above. Lysed pellets were centrifuged at 357,000 g for 10 min at 4°C and used for Pi measurements (cytosolic Pi). In order to determine the proportion of Pi released, the amount of Pi (in nmol) from each compartment (cytosol/extracellular milieu) was calculated using the appropriate dilution factors, then divided by the total amount of Pi measured in each sample (cytosol + extracellular milieu).

Glutamate uptake

COS7 cells expressing VGLUT 1, 2, or 3 and a MOCK control cell line were cultivated in 10 cm dishes as given above. After reaching 70%–80% of confluence, cells were washed twice and incubated for 20 min at 37°C with KREBS 4.7 mM [K+] (see Pi measurement). Following incubation, cells were collected and washed twice with glycine buffer (see Pi measurements) using centrifugation steps 900 g for 2 min at RT. Uptake (15 min at 37°C) was initiated by adding or not 10 mM [NaGlutamate] and/or 10 mM [NaPi] in uptake buffer. The reaction was stopped by quickly transferring the samples on ice, performing two quick washing steps with ice-cold glycine buffer and centrifugation (> 10,000 g for 30 s at 4°C). Cell pellets were then lysed in 250 μL sterile ice-cold water for 20 min while shaking at 1,000 rpm. Samples were centrifuged at 357,000 g for 10 min at 4°C. The glutamate content in the supernatant was determined by the addition of 2 μM of iGluSnFR A184S (a recently developed fluorescent glutamate sensor, kindly provided by L. Looger, HHMi Virginia USA) and the fluorescence changes were measured under excitation/emission at 495/520 nm, respectively (Marvin et al., 2018). The glutamate content was normalized to the number of cells per data point.

Immunofluorescence microscopy and immunoblots

Cell samples were washed twice in phosphate buffered saline (PBS) 0.1M, then fixed with PFA 4% for 10 min at RT. Samples were then washed three times in PBS/Triton X-100 (99.9/0.1%) and blocked in PBS/goat serum/Triton X-100 (89.9/10/0.1%) for 1h at RT on an oscillating plate. Incubation with primary antibodies was performed on an oscillating plate in PBS/goat serum/Triton X-100 (98.9/1/0.1%) overnight at 4°C with the dilutions indicated in the table. Cells were then washed three times with PBS/Triton X-100 (99.9/0.1%), and incubated with the secondary antibodies for 1 h at RT under agitation. Cells were washed three times, then mounted under coverslip using immumount, and stored at 4°C. Image acquisition was performed using a Leica LSM700 confocal microscope. Settings were adjusted for each antibody using immunopositive samples (e.g., COS7-VGLUT1 for VGLUT1 staining) and then kept for all samples derived from the same parent cell line (e.g., COS7-VGLUT1/2/3, and COS7-MOCK but not PC12-VGLUT1). PMT (Photomultiplier) amplifications were set to provide good signal/background ratio while avoiding pixel saturation.

Dilution of Antibodies

	Dilution	
Target	immunoblot	immunohisto
Primary antibodies		
eGFP	N/A	1/2,500
VGLUT1 (SLC17A7)	N/A	1/1,000
VGLUT1 (SLC17A7)	1/5,000	N/A
VGLUT2 (SLC17A6)	N/A	1/2,500
VGLUT2 (SLC17A6)	1/2,500	N/A
VGLUT3 (SLC17A8)	1/2,500	1/500
Synaptophysin	1/2,500	N/A
SV2A	1/2,500	N/A
GAPDH	1/4,000	N/A
PiT1 (SLC20A1)	1/1,000	N/A
PiT2 (SLC20A2)	1/1,000	N/A
Secondary antibodies		
anti-Rat Alexa 488	N/A	1/500
anti-Guinea pig Alexa 555	N/A	1/500
anti-Rabbit Cy5	N/A	1/500
anti-Rabbit HRP	1/2,000-1/10,000	N/A
anti-Mouse HRP	1/5,000-1/8,000	N/A
anti-Mouse (light chain) HRP	1/2,000	N/A

For immunoblot analysis, synaptosomes were prepared from the forebrain of fetal (e18), juvenile (P3, P5) or adult (P90) mice as described above. Samples were analyzed by sodium dodecyl sulfate-polyacrylamide gel electrophoresis (SDS-PAGE) and immunoblot techniques using the antibodies at dilutions displayed in the table and the ECL detection system.

Image treatment

Images were all acquired at a sensitivity range avoiding saturation and were occasionally enhanced in Photoshop CS6 (Adobe) using only linear conversions for figure preparation and conserving settings between related samples (e.g., all COS7-VGLUTs and COS7-MOCK).

QUANTIFICATION AND STATISTICAL ANALYSIS

Data are either shown as distribution plot (basal cytoplasmic levels of Pi i.e., samples incubated without Pi) or normalized to a control defined as no Pi for analysis of Pi uptake ± VGLUT inhibitor and 10 mM [Pi] in the absence of glutamate in the case of glutamate dose-response curves (Figures 4 and S4). Graphs present the mean of independent experiments ($2 \leq n \leq 22$), each condition being carried out in three to four replicates per experiment, and error bars figure SEM calculated from these independent experiments. All values were normalized to either synaptosomal protein content, cell number (10^3 cells), and/or standard conditions (no Pi or 10 mM [Pi] for uptake or inhibition studies, respectively). Inter-experimental variability is presented for each control condition as dot distributions in basal Pi (Figures 1, 2, S1, and S2) or glutamate content (Figure S3) figures.

Statistical significance was assessed using 2-tailed homoscedastic Student's modified t test. Significance is indicated as follows: ***$p < 0.001$, **$p < 0.01$, *$p < 0.05$, ns: not significant.

Numbers given in the figures indicate statistical significance (or not) of differences toward the following conditions:

(1) no Pi or no Glutamate. // (2) Pi. // (3) 4.7 mM [K+] control. // (4) 30 mM [K+] control. // (5) VGLUT2 KO control. // (6) VGLUT2 WT. // (7) VGLUT2 Het. // (8) no Dox. // (9) MOCK. // (10) Glut.